International Journal of Nanomedicine

Dovepress
open access to scientific and medical research

Open Access Full Text Article

ORIGINAL RESEARCH

Polyvinylpyrrolidone Assisted One-Pot Synthesis of Size-Tunable Cocktail Nanodrug for Multifunctional Combat of Cancer

Cheng Wang[1,*], Jiaoyang Pan[1,*], Shaoqing Chen[2], Lin Qiu[1], Huaanzi Hu[1], Li Ji[3], Jianhao Wang[1], Wenjia Liu[4], Xinye Ni[2]

[1]School of Pharmacy, Changzhou University, Changzhou, Jiangsu Province, People's Republic of China; [2]Department of Radiology, The Affiliated Changzhou No. 2 People's Hospital of Nanjing Medical University, Changzhou, Jiangsu Province, People's Republic of China; [3]Department of Otorhinolaryngology, The Affiliated Changzhou No. 2 People's Hospital of Nanjing Medical University, Nanjing, Jiangsu Province, People's Republic of China; [4]Department of Gastroenterology, The Affiliated Changzhou No. 2 People's Hospital of Nanjing Medical University, Changzhou, Jiangsu Province, People's Republic of China

*These authors contributed equally to this work

Correspondence: Wenjia Liu; Xinye Ni, Email 13813016290@126.com; nxy@njmu.edu.cn

Background: The in vivo barriers and multidrug resistance (MDR) are well recognized as great challenges for the fulfillment of antitumor effects of current drugs, which calls for the development of novel therapeutic agents and innovative drug delivery strategies. Nanodrug (ND) combining multiple drugs with distinct modes of action holes the potential to circumvent these challenges, while the introduction of photothermal therapy (PTT) can give further significantly enhanced efficacy in cancer therapy. However, facile preparation of ND which contains dual drugs and photothermal capability with effective cancer treatment ability has rarely been reported.
Methods: In this study, we selected curcumin (Cur) and doxorubicin (Dox) as two model drugs for the creation of a cocktail ND (Cur-Dox ND). We utilized polyvinylpyrrolidone (PVP) as a stabilizer and regulator to prepare Cur-Dox ND in a straightforward one-pot method.
Results: The size of the resulting Cur-Dox ND can be easily adjusted by tuning the charged ratios. It was noted that both loaded drugs in Cur-Dox ND can realize their functions in the same target cell. Especially, the P-glycoprotein inhibition effect of Cur can synergistically cooperate with Dox, leading to enhanced inhibition of 4T1 cancer cells. Furthermore, Cur-Dox ND exhibited pH-responsive dissociation of loaded drugs and a robust photothermal translation capacity to realize multifunctional combat of cancer for photothermal enhanced anticancer performance. We further demonstrated that this effect can also be realized in 3D multicellular model, which possibly attributed to its superior drug penetration as well as photothermal-enhanced cellular uptake and drug release.
Conclusion: In summary, Cur-Dox ND might be a promising ND for better cancer therapy.
Keywords: one-pot synthesis, size-tunable, multifunctional, cancer

Introduction

Cancer, characterized by uncontrolled cell growth and the potential to invade other tissues, poses a profound challenge in the realm of biomedical science and healthcare.[1–3] Cancer remains one of the most formidable diseases worldwide to date, accounting for an estimated 609,820 deaths in the United States alone in 2023.[4] Despite great advances have been achieved in the past decades with the development of various kinds of antitumor drugs, the efficacy of many clinically applied antitumor drugs upon in vivo application is often substantially compromised.[5,6] Recent studies have revealed that in vivo barriers and multidrug resistance (MDR) of cancer cells might contribute significantly to this drawback.[7,8] In vivo barriers encompass the complex physiological environment within living organisms that can impede the effective delivery and distribution of therapeutic agents to target cancer cells.[9] Factors such as the tumor microenvironment,[10] heterogeneous blood supply and drug metabolism,[11] and the presence of physiological barriers like the blood–brain barrier[12] contribute to the intricate landscape that influences drug accessibility and efficacy. Furthermore, MDR, a phenomenon where cancer cells develop

Received: 26 January 2024
Accepted: 30 April 2024
Published: 17 May 2024

Graphical Abstract

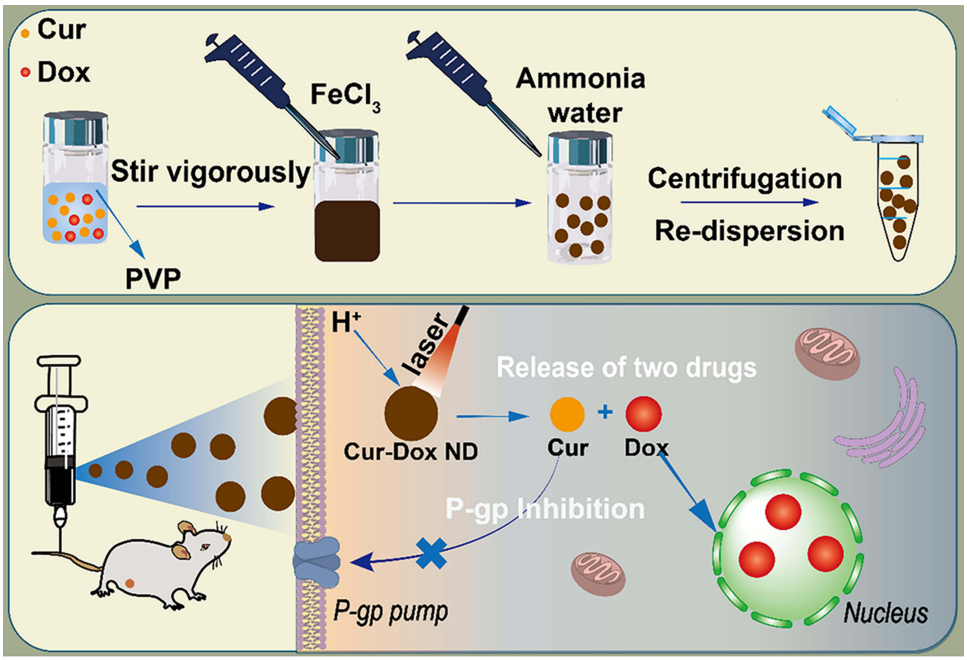

resistance to multiple drugs, also poses another significant hurdle.[13] This resistance can arise due to genetic mutations, overexpression of drug efflux pumps, and alterations in cellular signaling pathways. Overcoming these challenges calls for the development of novel therapeutic agents and innovative drug delivery strategies that can evade or overcome these barriers.

Drug delivery is the art and science of administering therapeutic agents to specific targets within the body. It involves designing and optimizing delivery systems to ensure precise dosing, targeted delivery, and controlled release of drugs. These systems can range from simple oral pills to sophisticated nanoparticles and implants. By enhancing drug stability, bioavailability, and tissue specificity, drug delivery technologies improve treatment efficacy while minimizing side effects.[14,15] The advent of nanodrugs represents a revolutionary approach for drug delivery in cancer treatment, offering distinct advantages in overcoming some of the longstanding challenges associated with conventional therapies.[16,17] Nanodrugs are engineered drug loaded particles on the nanometer that can specifically be delivered to cancer cells.[18,19] Their diminutive size allows for enhanced penetration and accumulation within tumor tissues, exploiting the abnormal vasculature associated with cancers.[20] This targeted delivery minimizes damage to healthy tissues and organs, mitigating the systemic side effects commonly observed with traditional chemotherapy.[21] Additionally, the unique physicochemical properties of nanodrugs enable sustained drug release, optimizing therapeutic concentrations over time.[22] The surface of these nanoparticles can be functionalized to enhance cellular uptake and improve their ability to evade biological barriers.[23] Moreover, nanodrugs provide opportunities for combination therapies, allowing for the co-delivery of multiple drugs or therapeutic modalities in a single nanoparticle system.[24] This versatility and precision make nanodrugs a promising frontier in cancer treatment, with the potential to bypass the in vivo barriers for enhancing therapeutic efficacy while minimizing adverse effects.

Addressing MDR in cancer treatment necessitates a multifaceted approach, and the significance of combination therapy as a potent countermeasure is getting increasing attention in recent years.[25] MDR often arises from the diverse mechanisms employed by cancer cells to evade the effects of individual drugs.[26] Combining multiple drugs with distinct modes of action can circumvent these resistance mechanisms and enhance therapeutic efficacy. Rational drug combinations, guided by a deep understanding of the molecular pathways involved in resistance, can target various vulnerabilities within cancer cells simultaneously while minimizing systemic toxicity.[27]

Moreover, the judicious use of nanodrug technologies can improve the selective delivery of therapeutic agents to tumor sites. This integrative and dynamic approach to combination therapy stands as a promising avenue in the ongoing battle against multidrug resistance in cancer. For example, a previous work presents a combination strategy of pretreatment of MDA-MB-231/MDR1 cells with quercetin followed by doxorubicin to overcome MDR.[28] The research suggests that the co-administration of natural compounds and chemotherapeutic drugs could be an effective strategy to combat MDR, which was also supported by other parallel studies.[29,30]

Photothermal therapy (PTT) stands as a promising way to revolutionize therapeutic strategies. PTT involves the use of light-absorbing agents, such as nanoparticles or organic dyes, which convert absorbed light into heat, selectively elevating the temperature of targeted cancer cells. This localized hyperthermia induces cellular damage and apoptosis, effectively eradicating cancer cells while minimizing harm to surrounding healthy tissues. The benefits of PTT lie in its specificity, and minimal invasiveness and convenience to combine with other modalities for multifunctional cancer therapy with improved overall therapeutic outcomes. It has been reported that PTT can improve the drug release[31] and drug penetration of nanoparticles,[32] as well as sensitize cancer cells to chemotherapy.[33] In many previous studies, the introduction of PTT can give significantly enhanced inhibition on tumor growth, which can even achieve full ablation of solid tumors.[34–36]

Although previous studies have shown the promise of multi-drug ND and PTT in cancer management, the integration of these functions into one drug delivery platform using a facile method is usually difficult as many previously reported NDs usually require complicated preparation procedures.[37,38] Here, in this study, with the aim to devise an ND platform to achieve enhanced anticancer effects, a size-tunable dual drug loaded ND was first developed by integrating curcumin (Cur) and doxorubicin (Dox) into the same ND (Cur-Dox ND) using ferric ion as the linker and PVP as the stabilizer and regulator. By changing the charge of Cur-Dox ND can be conveniently regulated ~10 nm to over 100 nm. The Cur-Dox ND can be responsive to both acidic tumor environment as well as photothermal to give enhanced anticancer performance (Scheme 1).

Materials and Methods

Materials

Doxorubicin hydrochloride (Dox), curcumin (Cur), indocyanine green (ICG), anhydrous ferric chloride, polyvinylpyrrolidone (PVP, K30 molecular weight: 44,000–54,000 Da), ammonia, methyl thiazolyl tetrazolium (MTT), verapamil and

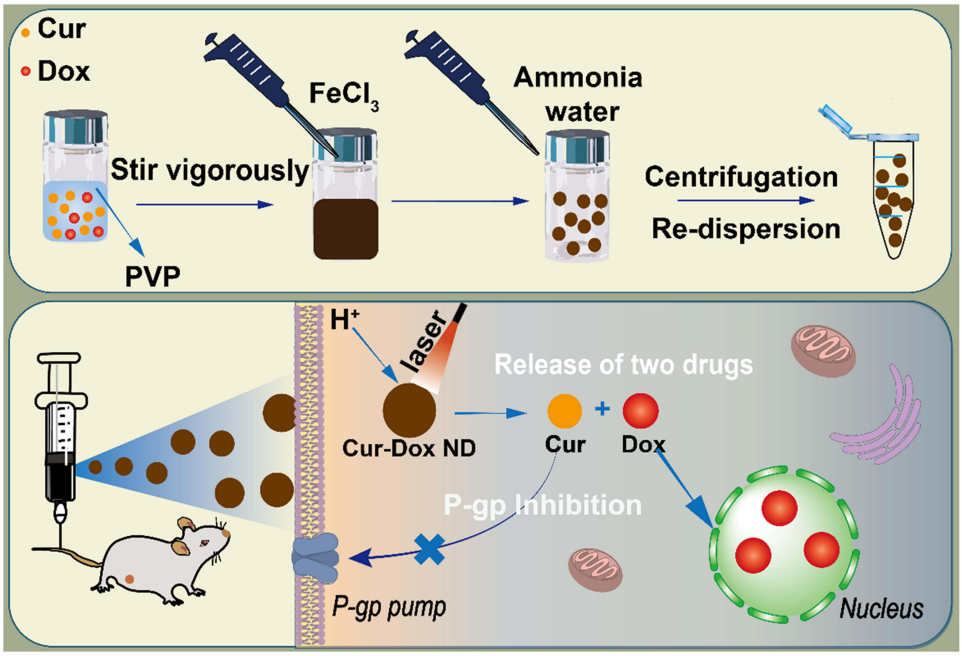

Scheme 1 The preparation and action mechanisms of Cur-Dox ND.

rhodamine 123 (Rh-123) were purchased from Adamas-beta Co., Ltd (Shanghai, China). Deionized (DI) water (Millipore Milli-Q grade, 18.2 MΩ) was used in all experiments. Other materials without specific statement were of analytical pure and provided by Adamas-beta Co., Ltd. Phosphate buffer saline (PBS) was purchased from Servicebio Co., Ltd (Wuhan, China). Fetal bovine serum, and Dulbecco's modified Eagle's medium (DMEM) were purchased from Thermo Fisher Scientific (Massachusetts, USA). Trypan blue (TPB) and calcein acetoxymethyl ester (Calcein-AM)/propidium iodide (PI) Double Stain Kit were purchased from Beyotime Biotechnology Co., Ltd (Shanghai, China).

Cell and Animal Models

The 4T1 (mouse breast cancer cell line) and NIH3T3 (mouse embryonic fibroblast) cells were obtained from Zhong Qiao Xin Zhou Biotechnology Co., Ltd (Shanghai, China). Cells were cultured in DMEM supplied with 10% FBS and placed in an incubator (Forma Direct Heat, Thermo Scientific, USA) at a temperature of 37 °C and atmosphere of 95% air/5% CO_2. Cells in the logarithmic phase were employed for experiments.

The multicellular tumor spheroid (MCTS) model was established according to the previous report.[32] In brief, a 96-well plate (Corning, USA) was individually covered with 50 μL of autoclaved agarose solution (2%, w/v) to give a gel matrix with concavity. Afterward, equally mixed 4T1 and NIH3T3 cells were seeded at a total density of 2×10^3 cells/well and cultured in standard conditions for 3–4 days to give MCTS.

Balb/c mice (female, 6–8 weak) were offered by Cavens animal center (Changzhou, China) and housed in SPF conditions with free access to food and water. The mice were subcutaneously injected with 50 μL of 4T1 cell suspension (4×10^7 cells/mL) at the flank. All subjects were returned to the above-mentioned feeding condition for the establishment of 4T1 tumor-bearing mouse model. All animal experiments were approved by the Animal Care and Use Committee of Changzhou University (No. 20220.0122) and conducted in Cavens animal center (Changzhou, China) in accordance with the guidelines for the care and use of laboratory animals.

Preparation of Cur-Dox ND

Dox, Cur, anhydrous ferric chloride, and PVP were dissolved separately in anhydrous ethanol. The feeding mass ratio was Dox:Cur:ferric chloride = 1:2:3 (2 mg:4 mg:6 mg), and the proportion of PVP was 10, 20, 25, 40, 50 μg per 10 mL ethanol solution. The solution of Dox, Cur, and PVP were mixed together, followed by quick adding of ferric chloride under vigorous stirring to initiate the reaction. After stirring for 10 min, 200 μL of aqueous ammonia was added to give precipitation. Cur-Dox ND was collected by centrifugation (12,000 rpm for 10 min), washed several times by DI water and then dispersed with an appropriate amount of DI water to give designated concentration. The probe sonication (ESW-650DN, Rongyi Instrument Co., Ltd, Shanghai, China) was used for the dispersion of Cur-Dox ND (80% power for 10 min in ice bath), followed by filtration through a 0.22 μm filter membrane to give the final nanoparticle dispersion. The single drug loaded nanodrug systems, PVP/Fe-Cur (Cur ND) and PVP/Fe-Dox (Dox ND), were synthesized using the same synthesis method with the same Dox and Cur feeds as in the preparation of Cur-Dox ND.

Characterization of Cur-Dox ND

The morphology of Cur-Dox ND was observed by transmission electron microscopy (TEM, Hitachi H-7800, Japan). The hydrodynamic size and zeta potential were tested using a Malvern Zetasizer Nano analyzer (ZS90, Malvern Instrument Co., Ltd, Malvern, UK). The particle size of Cur-Dox ND dispersed in saline was monitored at room temperature for 15 days, while that in DMEM containing 10% FBS was monitored at 37 °C for 12 h. The fluorescence/UV-vis spectrum and absorption of nanoparticles was recorded by fluorescence spectrophotometer (FS5, Edinburgh Instruments Ltd., UK) and UV–vis spectrophotometer (Spectrumlab 53, Lengguang technology Co., Ltd, Shanghai, China), respectively. The Fourier transform infrared (FTIR) spectrum of Cur-Dox ND, Dox, PVP, and Cur was characterized using FTIR spectroscopy (Nicolet™ iS20, Thermo Scientific Ltd. US).

The photothermal effect of Cur-Dox ND was tested by recording the solution temperature every 30s upon irradiating by 808 nm laser for a duration of 5 min at various laser power (1, 2, 2.5 W), nanoparticle concentration fixed at 0.4 mg/mL and concentrations (0.05, 0.1, 0.2, 0.3 and 0.4 mg/mL, laser power fixed at 2 W).

Hemolysis assay was conducted according to previous report.[39] In brief, different concentrations of Cur-Dox ND (3, 6, 12, 24, 48, 96, 192 μg/mL) were incubated with 2% red blood cells suspension of Balb/c mice at 37 °C for 1 h, followed by centrifugation (1500 rpm, 5 min) to remove cells. The supernatant was measured by recording UV–vis absorbance at 545 nm. Red blood cells incubated with PBS and 1% Triton X-100 were selected as 0% and 100% hemolysis, respectively.

The pH-responsive drug release of Cur-Dox ND was assessed using dialysis method. In brief, 1 mL of freshly prepared Cur-Dox ND (containing 830 μg/mL Dox) was loaded into a dialysis bag (3500 Da) and placed in 15 mL of PBS (pH 7.4 and 5.5, containing 0.5% of Tween 80). The entire system was then placed in a transdermal diffusion apparatus (TP6, Jingtuo Instrument Technology Co., Ltd, Tianjin, China) at 37 °C and 100 rpm. The Dox concentration in the release medium was determined by measuring the excitation at 590 nm using fluorescence spectrophotometer.

Cellular Uptake of Cur-Dox ND

The 4T1 cells were seeded into 24-well plates at 1×10^5 per well for 12 h, followed by incubation with Cur-Dox ND at the Dox concentration of 2 μg/mL. At designated time points (0.5, 2, 4, 8, 12, 24 h), the intracellular Dox signal was quantitatively analyzed by flow cytometry (C6 Plus, BD Accuri Co., Ltd, Shanghai, China). Under the same experimental conditions, the cells were divided into three groups: free Dox, Cur-Dox ND, Cur-Dox ND+Laser. In the group of Cur-Dox ND+Laser, 4T1 cells were co-incubated with Cur-Dox ND for 1 and 2 h, respectively, followed by irradiation with an 808 nm near-infrared laser for a duration of 10 min. Subsequently, the cells were held under incubation for an additional 1 h, and then cells were stained with DAPI. Uptake of the drug by the cells was observed using a confocal laser scanning microscope (CLSM Ti2, Nikon eclipse Co., Ltd, Japan).

In vitro Cytotoxicity

The 4T1 cells were seeded in 6-well plates with 2×10^5 cells per well for 12 h. Afterwards, cells were incubated with Cur-Dox ND under different concentration gradients (5,10, 20 μg/mL) and pHs (pH 7.4, 5.5) for 24 or 48 h. In parallel, cells were subjected to NIR laser irradiation (808 nm, 2 W, 5 min) after incubation with Cur-Dox ND at pH 7.4 for 4 h, followed further incubation for 20 h. Afterward, all cells in the culture plate were collected and evenly dispersed in DMEM. The cell suspension was then incubated with trypan blue dye at 37 °C for 3 min, and cell viability was assessed using a cell counter (C100&C100-SE, RWD Life Science Co., Ltd, Shenzhen, China).

In parallel, 4T1 cells were seeded in 96-well plates with 8×10^3 cells per well for 12 h and subjected to the same treatment as mentioned above. At the end of the experiment, the cell viability was assessed using MTT assay.

In parallel, 4T1 cells were seeded in 24-well plates with 1×10^5 cells per well for 12 h, followed by staining by Calcein AM/PI Double Stain Kit according to manufacturer's instructions. The image was captured by fluorescence inverted microscope (Ti–S, Nikon Corporation, Tokyo, Japan).

MCTSs with diameters of 300–400 μm were divided into four groups (n = 3): (1) Control; (2) Dox ND; (3) Cur-Dox ND; (4) Cur-Dox ND+Laser. The selected spheroids were treated with fresh medium containing Cur-Dox ND and Dox ND (Dox concentration 2 μg/mL). The MCTS in Cur-Dox ND+Laser group underwent daily exposure to an 808 laser at a power of 2 W for a duration of 5 min. The volume of MCTS was recorded for 7 days.

Drug Penetration Study

The MCTS was incubated with free Dox or Cur-Dox ND at the Dox concentration of 3 μg/mL for a duration of 24 h. Afterwards, the spheroids were aspirated and placed on a slide. The images of the tumor spheroids were acquired by tomoscan using Z-stack imaging with 25 μm intervals from the middle of the spheroid to the bottom by CLSM.

P-Gp Inhibition

4T1 cells were seeded into 24-well plates at 1×10^5 per well for 12 h in 5% CO_2 under 37°C. The cells were treated with Rh-123 for 4 h, then replaced with Cur-Dox ND, Dox ND, Dox (Dox concentration of 20 μg/mL) or verapamil (10 μg/mL) contained fresh medium for an additional 8 h of incubation. Thereafter, different groups of cells were tested for green fluorescence intensity using a flow cytometer. Cells were subjected to the same treatment and observed under a laser scanning confocal microscope.

Biodistribution

Firstly, a suspension containing approximately 2×10^6 4T1 cells was subcutaneously injected into the dorsal region of BALB/c mice to establish the 4T1 tumor-bearing mice. Subsequently, free ICG and ICG labeled Cur-Dox ND were intravenously injected into model mice. At prearranged time intervals (1, 2, 4, 8, 12, 24, 48 h), the distribution of fluorescence signal within the mice was recorded by small animal live imaging system (Tanon X6, Shanghai, China). After living imaging, one mouse was sacrificed, and the main organs and tumor tissues were excised for ex vivo imaging using the same imaging system.

In vivo Antitumor Assay

The 4T1 tumor-bearing mice with a tumor volume around 120 mm^3 were randomly divided into four groups (n = 5) and treated with saline, Dox ND or Cur-Dox ND (Dox dosage: 4.5 mg/kg) every other day for 14 days. In parallel, mice administered with Cur-Dox ND were subjected to 808 nm NIR laser irradiation, at the power of 2 W for a duration of 5 min (denoted as Cur-Dox ND+Laser group). PTT was conducted at 4 h after drug administration for 4 times. The tumor volumes of all subjects were recorded before drug administration. The mice were sacrificed at the end of the test, and the tumor tissues of the subjects were obtained for physiopathological analysis using H&E and Ki67 staining.

Statistical Analysis

Statistical analysis was performed using GraphPad Prism 8 or Origin 2022, with statistical significance calculated using *T*-test. A statistically significant difference was considered when $P < 0.05$.

Results and Discussion

Preparation of Cur-Dox ND

According to our previous research and literatures, ferric is a powerful chelating ion which is capable of complexing molecules with phenol groups.[36,40] However, different from these studies, we introduced PVP, which is a widely adopted biomedical material, as both stabilizer and regulator for the synthesis of Cur-Dox ND. The unique properties of PVP, including high solubility in water and many organic solvents, biocompatibility, and non-toxicity, make it an essential component in pharmaceutical science. PVP is a good stabilizer in to enhance drug solubility and bioavailability. PVP's ability to complex with various substances also makes it valuable in the stabilization of colloidal systems. Importantly, we revealed that the particle size of the final product can be finely tuned by adjusting the charged ratio of PVP. As shown in Figure 1A, the particle size of the product is negatively related to the ratio of PVP, which can range from ~10 nm to over 100 nm. It was also noted that the dispersions of size for these particles are all narrowly located in a small range, indicating the well dispersion of the nanoparticles. This is a valuable discovery as previous studies have shown the critical role of size in influencing the in vivo fate of nanoparticles, thus determining the final antitumor performance.[41,42] Therefore, it was suggested that the PVP assisted size control synthesis of nanoparticles in this study can be a powerful tool in designing suitable drug delivery system for better cancer treatment, which deserves our future investigations.

In order to fully reveal the potential of Cur-Dox ND, we selected the product with size of 20 nm as the model ND and proceeded with the following assays. The detailed size distribution and morphology observation results of the selected Cur-Dox ND are shown in Figure 1B and C, respectively. The results in Figure 1C revealed that Cur-Dox ND is near spherical particles with size around 20 nm and good dispersion, which is consistent with that reported in Figure 1B. The surface charge of the selected Cur-Dox ND is almost neutral (Figure S1), which might relate to the modification of PVP on the nanoparticle surface. To verify the successful loading of both drugs into Cur-Dox ND, the color changes before and after the reaction were recorded. As shown in Figure S2, the solutions of $FeCl_3$ and Cur are yellow, while that of Dox is red. However, after reaction, the resultant Cur-Dox ND dispersion was turned into black. The significant changes in color indicated the forming of new substances. In order to verify this suggestion, the UV–vis spectrum of Cur, Dox and Cur-Dox ND was recorded. As shown in Figure 1D, the peaks of Dox ND (~300 nm) and Cur ND (~400 nm) still preserved in the UV–vis spectrum of Cur-Dox ND, indicating the loading of both drugs in the same ND platform. From the FTIR results in Figure 1E, we can see that the

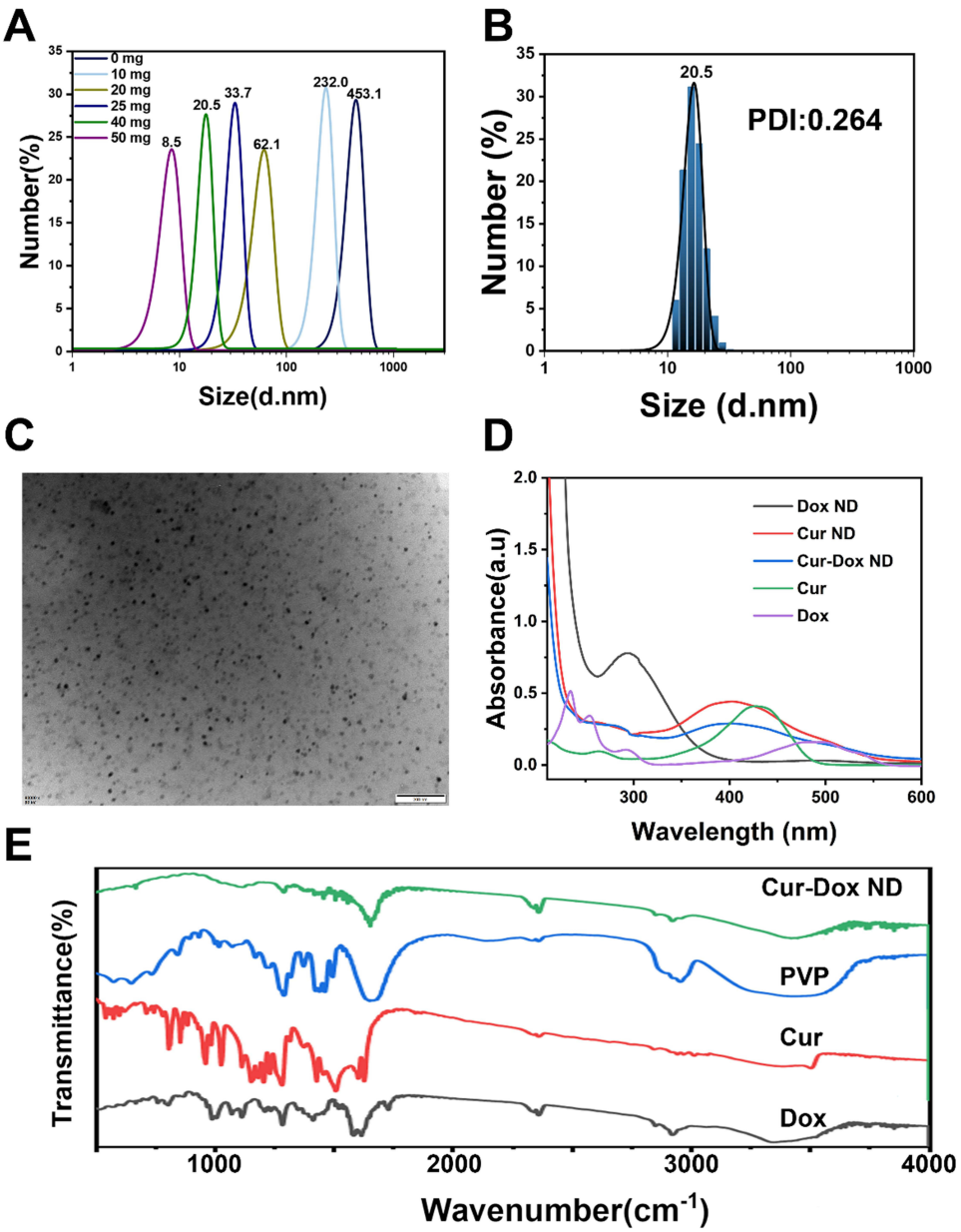

Figure 1 Preparation and characterization of Cur-Dox ND. (**A**) The size-controllable preparation of Cur-Dox ND by adjusting the ration of PVP. The size distribution (**B**) and TEM image (**C**) of selected Cur-Dox ND. Scale bar is 200 nm. (**D**) The UV-vis spectrum (**D**) and FTIR spectrum (**E**) of different raw materials or NDs.

characteristic peaks of PVP can also be observed in that of Cur-Dox ND. Therefore, results from Figure 1D and E suggested the successful integration of all three components (Cur, Dox and PVP) into Cur-Dox ND.

Here in our study, the loading of two different drugs into Cur-Dox ND can be facilely achieved using a one-pot method with high reproducibility, which is of significant importance for its further advance into clinical practice and even large-scale production.

Synergetic Chemotherapy of Cur-Dox ND

After confirming the successful loading of both drugs into Cur-Dox ND, we next aim to test if both drugs can still exert their functions on the same target cell. Cur is a natural polyphenol derived from turmeric. Previous reports have indicated that Cur holds great potential in reversing MDR in cancer cells by modulating key cellular pathways and inhibiting drug efflux pumps, thereby enhancing the efficacy of conventional chemotherapy.[43,44] To substantiate the synergistic

anticancer potency of Cur and Dox in Cur-Dox ND, single drug loaded ND, ie, Cur ND and Dox ND were separately synthesized. Subsequent investigative analyses involved the implementation of TPB staining assay, MTT assay, and live/dead cell staining experiment to assess the inhibitory impact of the three distinct NDs on 4T1 cells. Cells exhibiting normal vitality with an intact cell membrane structure have the ability to repel TPB, preventing its entry into the cell. In contrast, cells that are inactive or incomplete experience an elevation in cell membrane permeability, leading to their staining in blue by TPB.

TPB assay (Figure 2A) showed no significant inhibitory effect of Cur ND on 4T1 cells, while that of Dox ND was not even reach IC50 even at the Dox concentration of 20 μg/mL, which suggested the high resistance of 4T1 cells to Dox. However, after treatment with Cur-Dox ND, the survival rate of 4T1 cells was significantly lower as compared to separate administration of Dox ND or Cur ND. This result provides primary conclusion that both loaded drugs in Cur-Dox ND can fully exert their functions to give increased anticancer performance. The MTT assays in Figure 2B also give consistent results. In this study, we employed the calcein AM and propidium iodide (PI) live/dead cell staining method to observe the cellular viability profile. Calcein AM induces robust green fluorescence in viable cells upon esterase cleavage, while PI elicits red fluorescence in nonviable cells by intercalating into the DNA double helix after penetrating disordered regions.[45] As depicted in Figure 2C, the augmentation of drug concentration resulted in a gradual reduction in green fluorescence intensity, accompanied by a concomitant rise in red fluorescence. As expected, Cur-Dox ND group showed much more significant increase in PI signal with the increase with drug concentrations than single drug loaded NDs.

The transmembrane protein P-glycoprotein (P-gp), coded by the multidrug resistance 1 (MDR1) gene, assumes a pivotal role in the manifestation of MDR within cancer cells.[46] To evaluate the inhibitory potential of Cur-Dox ND on P-gp, a Rh-123 inhibition experiment was conducted. Rh-123, a widely used P-gp substrate with green fluorescence,

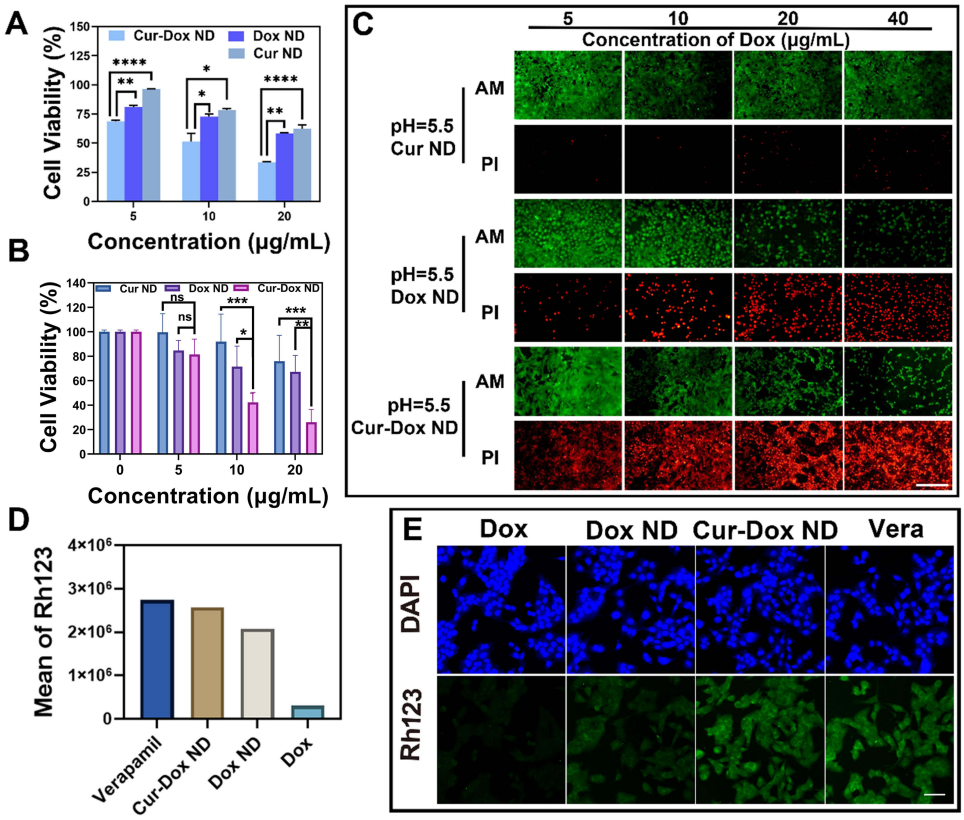

Figure 2 Synergetic chemotherapy of Cur-Dox ND. Cell viability of 4T1 cells treated with different concentration of NDs for 48 h using TPB staining assay (**A**) and MTT assay (**B**). Data were presented as mean ± SD, n = 4. (**C**) Fluorescent image of 4T1 cells stained with Calcein-AM (green, live cells) and PI (red, dead cells). Scale bar is 200 μm. Quantitative (**C**) and qualitative (**E**) analysis of fluorescence signal of Rh-123 in different groups using flow cytometry and CLSM, respectively. Scale bar is 50 μm. (1–4* represent *t*-test, ns: no significance, $P < 0.01$, $P < 0.005$, $P < 0.001$, $P < 0.0001$ respectively).

served as an indicator for P-gp inhibition and drug efflux. As a positive control, verapamil, a recognized P-gp inhibitor, was employed.[47] Following the equal uptake of Rh-123 and subsequent treatment with different formulations, both Cur-Dox ND and verapamil groups displayed elevated levels of intracellular Rh-123 compared to other groups. These observations were consistent with results obtained through flow cytometry analysis of 4T1 cells (Figure 2D) and CLSM imaging (Figure 2E). Notably, the intracellular retention of Rh-123 in cells treated with Cur-Dox ND surpassed that of free Dox. Additionally, flow cytometry investigations into cellular uptake revealed a time-dependent pattern for Cur-Dox ND in 4T1 cells (Figure S3). Approximately 34.29% uptake was observed at 0.5 h, increasing steadily even after 24 h, suggesting both rapid uptake and prolonged retention of Cur-Dox ND. Importantly, the uptake of Cur-Dox ND by 4T1 cells was significantly more rapid and substantial compared to the uptake of free Dox at an equivalent concentration.

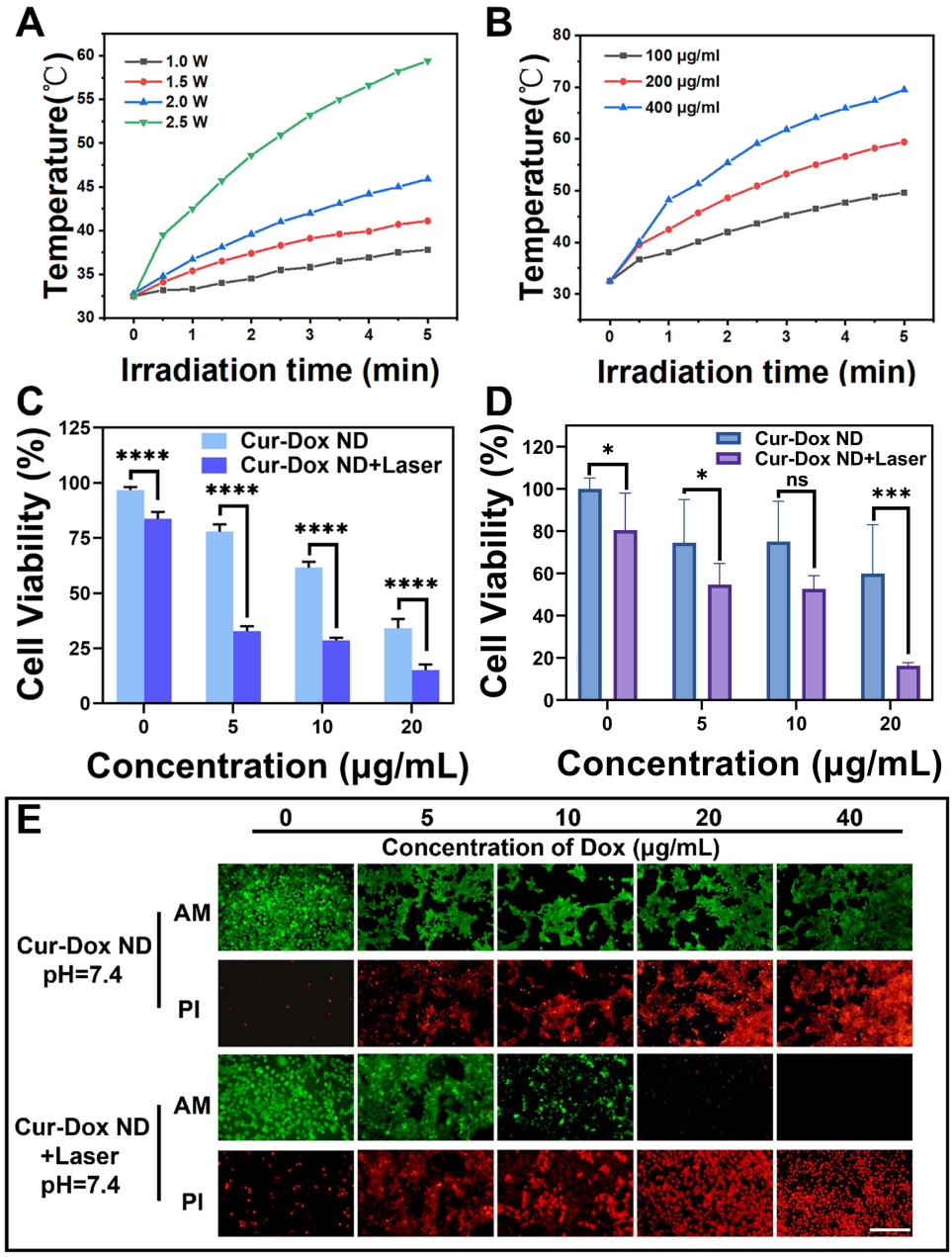

Figure 3 Photothermal properties of Cur-Dox ND and photothermal enhanced antitumor efficacy in vitro. Temperature elevation of Cur-Dox ND solutions under different laser power (**A**) and different concentrations (**B**). Cell viability of 4T1 cells treated with different concentration of Cur-Dox ND with or without laser irradiation for 24 h using TPB staining assay (**C**) and MTT assay (**D**). Data were presented as mean ± SD, n = 4. (**E**) Fluorescent image of 4T1 cells stained with Calcein-AM (green, live cells) and PI (red, dead cells). Scale bar is 200 μm. (1–4* represent *t*-test, ns: no significance, $P < 0.01$, $P < 0.005$, $P < 0.001$, $P < 0.0001$ respectively.).

These findings are in accordance with prior reports, indicating that ND can counteract drug resistance by utilizing different cellular entry pathways.[25,48] It is noteworthy that the verapamil group exhibited the highest Rh-123 retention, followed by the Cur-Dox ND group, which was markedly higher than that of the Dox ND group. These results further validate the complete realization of the P-gp inhibition effect of Cur within Cur-Dox ND upon administration, effectively collaborating with Dox to reverse MDR and achieve enhanced inhibition of 4T1 cancer cells.

Responsive Therapeutic Activities of Cur-Dox ND

Responsive drug delivery is a cutting-edge approach in the field of pharmaceutical science which is designed to dynamically adapt to the changing conditions and respond to various stimuli such as changes in pH, temperature, enzymatic activity, or specific biomarkers.[49] The concept behind responsive drug delivery is to enhance drug efficacy while minimizing side effects by ensuring precise and targeted drug release, making it a forefront area of research with the potential to revolutionize the regime of cancer therapy.[50] As a result, the responsive performances of Cur-Dox ND upon different pH conditions and laser irradiation were tested. The stability of Cur-Dox ND under normal physiological environments was firstly assessed. As shown in Figure S4, the size as well as polydispersity index (PDI) of Cur-Dox ND in saline maintained stable during storage under room temperature for 15 days. More importantly, both parameters for Cur-Dox ND also showed inconspicuous changes in FBS for at least 12 h. These results collectively proved the good stability of Cur-Dox ND upon storage and in vivo applications. However, when incubated under acidic environments, as demonstrated in Figure S5, the size of Cur-Dox ND suffered from significant change to over 1000 nm, indicating its instability under acidic tumor environments.

To cope with metabolic acidosis, cancer cells exhibit an overexpression of pH regulators on their surface, facilitating the expulsion of excess protons/lactic acid and consequently acidifying the tumor microenvironment.[51] While the pH levels in normal human tissue typically hover around 7.4, tumor tissue tends to exhibit a lower pH, ranging from 6.8 to 5.0.[52] Hence, the development of ND capable of releasing loaded drugs in response to the acidic tumor environment is recognized as a crucial advantage in drug delivery strategies.[53]

In the fluorescence spectrum of Cur-Dox ND, the distinctive absorption peak of Dox at 590 nm diminishes, indicating fluorescence quenching resulting from the complexation of Dox with metal ions. This decline in fluorescence is attributed to the formation of non-emissive ground-state complexes.[54] However, upon exposure to an acidic solution, the characteristic DOX peak re-emerges, suggesting that Cur-Dox ND has the ability to release drugs under acidic conditions (refer to Figure 4A).

In this study, depicted in Figure 4B, we examined the release dynamics of Cur-Dox ND in vitro, utilizing PBS buffer solutions with pH conditions of 7.4 and 5.5. The release rates and durations were monitored over a span of 72 h. Notably, at pH 7.4 and 5.5, the release rates were 34.79% and 54.87%, respectively. A discernible increase in Dox release rate was observed with decreasing pH, surpassing 50.00%. These results affirm the pH-sensitive nature of Cur-Dox ND, showcasing its capability for sustained release in tumor tissues, thereby facilitating enduring anticancer effects.

To validate this phenomenon, we conducted cell viability tests on 4T1 cells following incubation with Cur-Dox ND at varying pH levels. As illustrated in Figure 4C, an inverse relationship between cell survival rate and concentration was evident. Moreover, a notable decrease in cell survival rate was observed in the pH = 5.5 group compared to the pH = 7.4 group at equivalent concentrations. Further validation of the tumor-suppressive effect of the pH-responsive Cur-Dox ND was performed using MTT assays to corroborate TPB staining results. As depicted in Figure 4D, in alignment with TPB staining outcomes, the MTT assay revealed significantly reduced cell viability at pH 5.5 compared to pH 7.4. In Figure 4E, concentration-dependent cell death was observed, particularly pronounced in the pH 5.5 group. These results visually substantiate the findings of both the MTT assay and TPB staining, supporting the conclusion that in an acidic environment, the liberated drugs from Cur-Dox ND intensify the inhibitory impact on tumor growth.

Furthermore, the photothermal transduction capability of Cur-Dox ND was evaluated. As illustrated in Figure 3A and B, a direct correlation between the concentration of Cur-Dox ND and its temperature was observed, with increased laser power enhancing this effect at a given concentration. These findings highlight the exceptional efficiency of Cur-Dox ND in both light absorption and heat conversion, positioning it as a promising candidate for controllable PTT. Given that previous studies have indicated that the incorporation of PTT can significantly augment the anticancer efficacy of chemotherapy,[55,56] we aimed to investigate whether the photothermal effects of Cur-Dox ND could enhance its ultimate anticancer performance. Results from

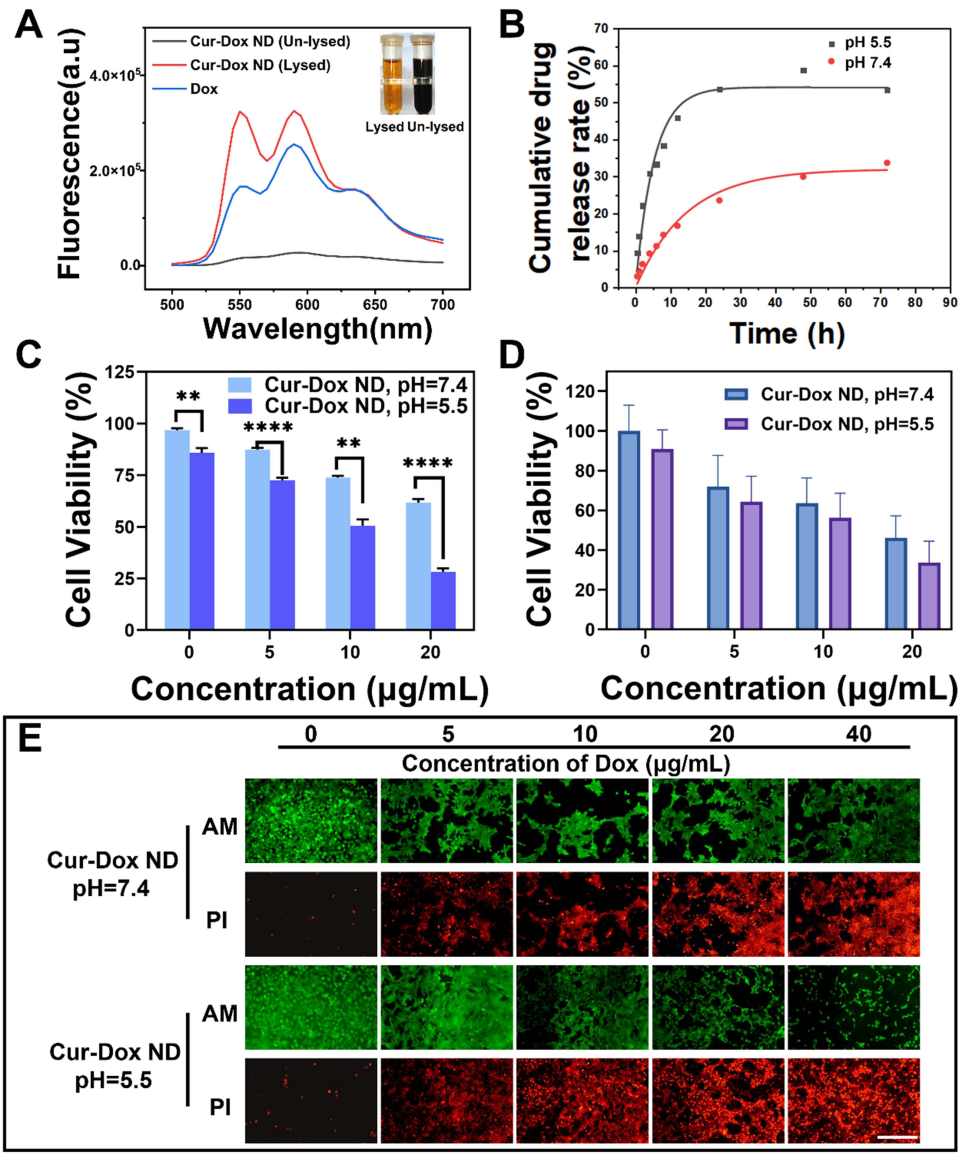

Figure 4 The pH-responsive antitumor efficacy of Cur-Dox ND in vitro. (**A**) Fluorescence spectrum of un-lysed Cur-Dox ND, lysed Cur-Dox ND and free Dox. (**B**) Release profiles of Dox from Cur-Dox ND at pH 5.5 and pH 7.4. Cell viability of 4T1 cells treated with different concentration of Cur-Dox ND under different pHs for 48 h using TPB staining assay (**C**) and MTT assay (**D**). Data were presented as mean ± SD, n = 4. (**E**) Fluorescent image of 4T1 cells stained with Calcein-AM (green, live cells) and PI (red, dead cells). Scale bar is 200 μm. (1–4* represent *t*-test, $P < 0.01$, $P < 0.005$, $P < 0.001$, $P < 0.0001$ respectively.).

the TPB staining experiment are presented in Figure 3C. In the non-photothermal group, varying concentrations of Dox yielded cell survival rates ranging from 77.75% to 34.00%. In contrast, the photothermal group exhibited markedly lower cell survival rates, ranging from 32.75% to 15.00% for the corresponding Dox concentrations. These outcomes strongly suggest that PTT substantially enhances the anticancer effect of chemotherapy. This conclusion is further substantiated by the MTT assay and live/dead cell staining experiment depicted in Figure 3D and E, respectively. These experiments provide compelling evidence affirming the potent multifunctional anticancer effects of Cur-Dox ND.

In vitro Combat of 3D Tumor and Potential Mechanisms

Tumor formation is often accompanied by changes in the surrounding connective tissue and matrix, as well as the development of the tumor microenvironment. Cancer cells cultured on plates cannot fully reflect the 3D structure of solid tumors. Therefore, in recent years, the MCTS is widely adopted to assess the in vitro antitumor performances of ND.[57,58]

To further validate the multifunctional anticancer effects of Cur-Dox ND nanoparticles, we evaluated their cytotoxicity on an MCTS model in vitro. The treatment scheme is presented in Figure 5A, and the results were supplied as Figure 5B and C. In contrast to the control, which exhibited continuous growth of MCTS volume, the group treated with Cur-Dox ND with laser irradiation demonstrated the strongest cytotoxicity with a significant reduction in MCTS volume at the culmination of the test. Compared with the other groups of tumor spheres, the cells in the photothermal group were significantly looser. By day 7, most of the cells had died, and cell debris was scattered nearby, suggesting the potential of this therapeutic approach in cancer treatment.

The outcomes of this study underscore the potent inhibitory effects on cancer demonstrated by a multifunctional therapeutic approach within a 3D tumor model. These effects surpass a simple explanation based on the synergistic mechanisms outlined in the above results. Consequently, our initial exploration focused on evaluating the drug penetration capabilities within these two treatment groups. The penetration of DOX fluorescence at various depths within the MCTS was systematically examined and

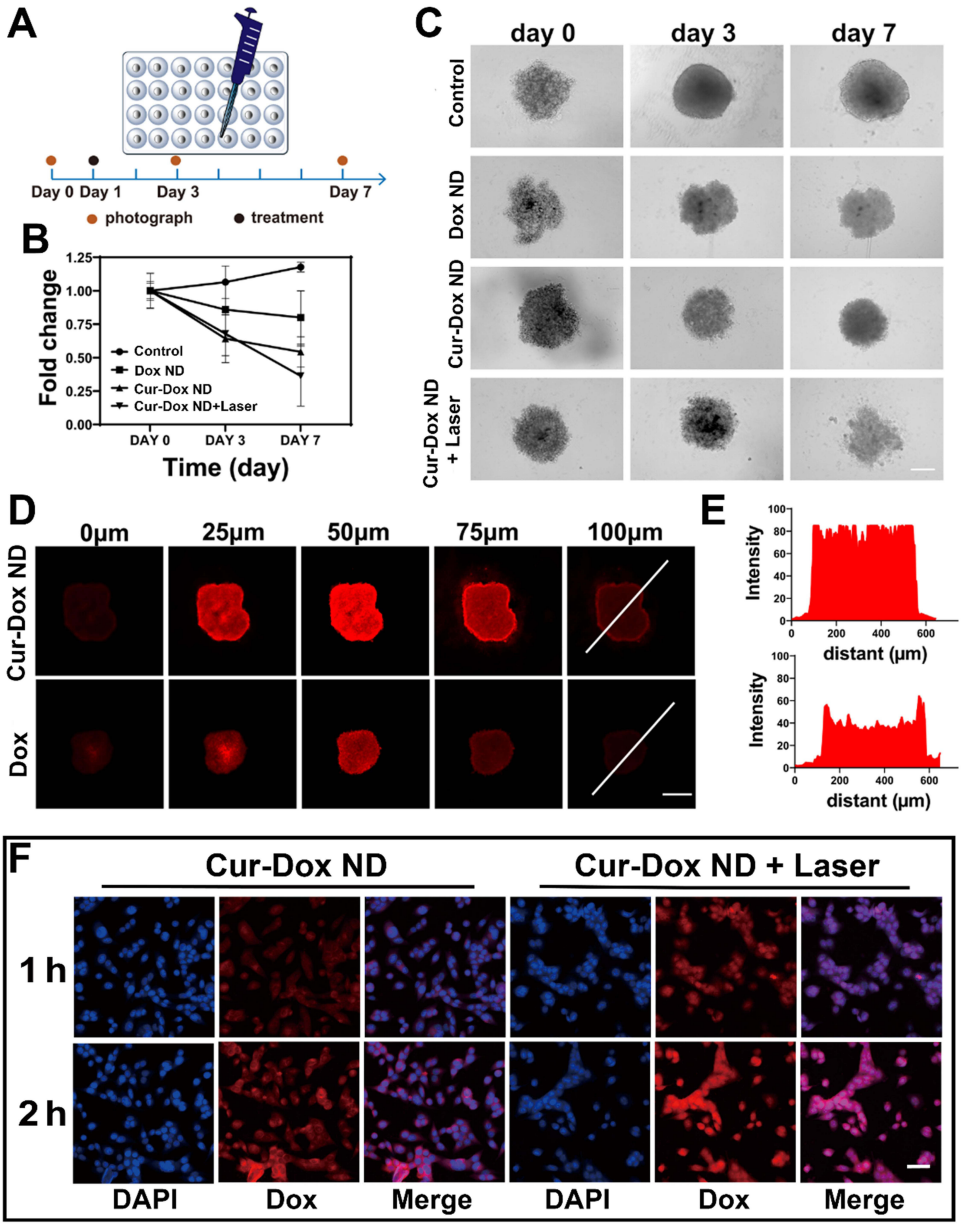

Figure 5 In vitro antitumor efficacy and mechanism on 3D MCTS model. (**A**) Treatment scheme of the experiment. Optical images (**B**) and corresponding analysis results summary (**C**) of MCTS after treatment with different formulations, Scale bar is 200 μm. Data were presented as mean ± SD, n = 4. Drug penetration imaging (**D**) and Dox signal distribution summary (**E**) of MCTS treated with Cur-Dox ND and free Dox. Scale bar is 300 μm. (**F**) Co-localization of drugs in 4T1 cells with or without laser irradiation at different time points. Scale bar is 50 μm.

recorded using CLSM. Notably, the Cur-Dox ND group exhibited profound drug penetration into the MCTS, evident from the discernible Dox signal at the central region of the tumor sphere, as depicted in Figure 5D and E. In contrast, the free Dox group, under identical conditions, exhibited accumulation predominantly at the periphery of the MCTS, with a notable decrease in intensity beyond a depth of 100 μm. Additionally, to gain deeper insights into the photothermal effects contributing to enhanced anticancer performance, we investigated the drug uptake and distribution in 4T1 cells following NIR laser irradiation. Figure 5F illustrates a significant augmentation in the cellular uptake of Cur-Dox ND upon laser irradiation, accompanied by a substantial increase in the Dox signal within 4T1 cells. Remarkably, the photothermal treatment induced a substantial accumulation of red fluorescence from DOX primarily localized within the cell nuclei, underscoring the efficacy of photothermal effects in augmenting Cur-Dox ND drug release. This aligns with previous findings suggesting that free Dox is more likely to enter cell nuclei.[59]

In vivo Tumor Targeting

The near-infrared dye ICG was encapsulated into the ND to investigate the in vivo distribution of Cur-Dox ND. In the cohort receiving the free ICG solution, fluorescence was predominantly observed in the liver and spleen post-intravenous injection, with only a faint fluorescent signal detected in the tumor tissue. Conversely, in the group administered ICG/Cur-Dox ND, distinct fluorescence was evident in the tumor area 4 h post-injection. Notably, at the 48-hour mark following administration, robust fluorescence persisted in the tumors, indicating the substantial accumulation and retention of Cur-Dox ND in the tumor tissue (see Figure 6). Collectively, these findings underscore the exceptional passive targeting capability of Cur-Dox ND toward tumor

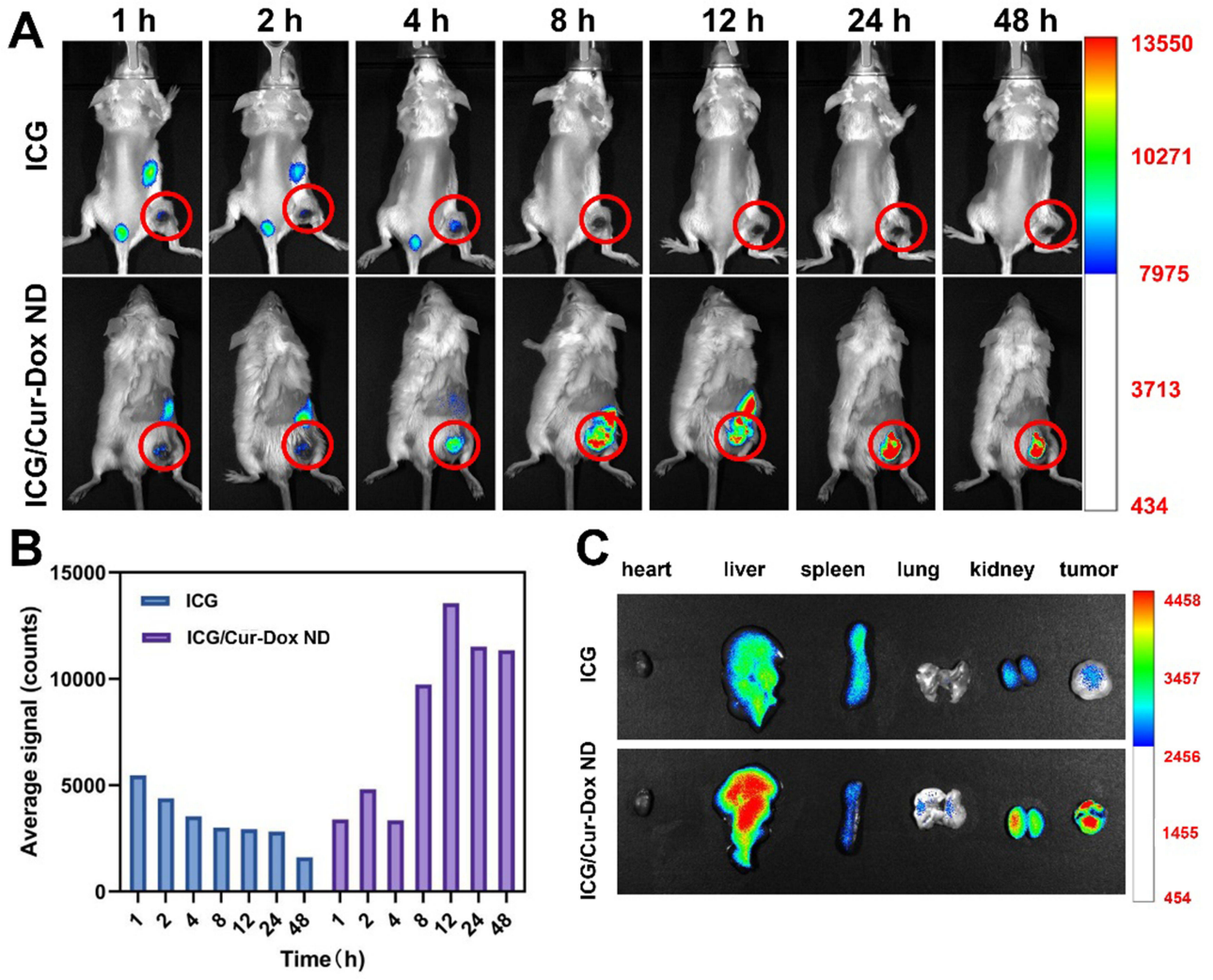

Figure 6 In vivo tumor targeting assay of Cur-Dox ND in 4T1 tumor-bearing Balb/c mice. Real time fluorescence image (**A**) and semiquantitative (**B**) of the in vivo distribution of ICG signal in different groups. (**C**) Ex vivo fluorescence images of major organs and tumors after intravenous injection of Cur-Dox ND for 48 h.

tissues. The substantial accumulation of Cur-Dox ND at tumor sites establishes a crucial foundation for multimodal treatment, particularly in the context of combinational PTT.

In vivo Antitumor Performance

In this investigation, we assessed the therapeutic efficacy of Cur-Dox ND in female Balb/c mice bearing 4T1 tumors. The mice were randomly allocated into four groups (n = 5): (1) normal saline, (2) Dox ND, (3) Cur-Dox ND, and (4) Cur-Dox ND+Laser, and subjected to distinct treatment regimens as outlined in Figure 7A. Analysis of the results depicted in Figure 7B revealed that the normal saline group exhibited the most rapid and substantial increase in tumor volume. Conversely, the Dox ND and Cur-Dox ND groups displayed a comparatively slower rate of tumor volume growth, with the Cur-Dox ND group showing a slightly smaller tumor size than the Dox ND group. Notably, the Cur-Dox ND+Laser group, receiving combined chemotherapy and PTT, demonstrated a remarkable treatment effect. The tumor volume showed no increase, and by the end of the treatment cycle, the tumor had completely regressed. Compared with many previous drug delivery platforms that can only retard the growth of tumors, our results underscore the favorable outcome of the synergistic application of chemotherapy and PTT in tumor treatment.[60,61] Multimodal therapy, in comparison to chemotherapy alone, exhibited a significantly enhanced tumor eradication effect.

Following the completion of in vivo experiments, the mice were euthanized, and tumor tissues from each group were collected for histological examination using H&E and Ki67 staining (Figure 7C). H&E staining results indicated that the tumor cells in the Cur-Dox ND group exhibited the highest degree of necrosis compared to other groups. Furthermore, Ki67 staining revealed that tumor cells in the Cur-Dox ND group displayed the lowest proliferation rates among all tested groups.

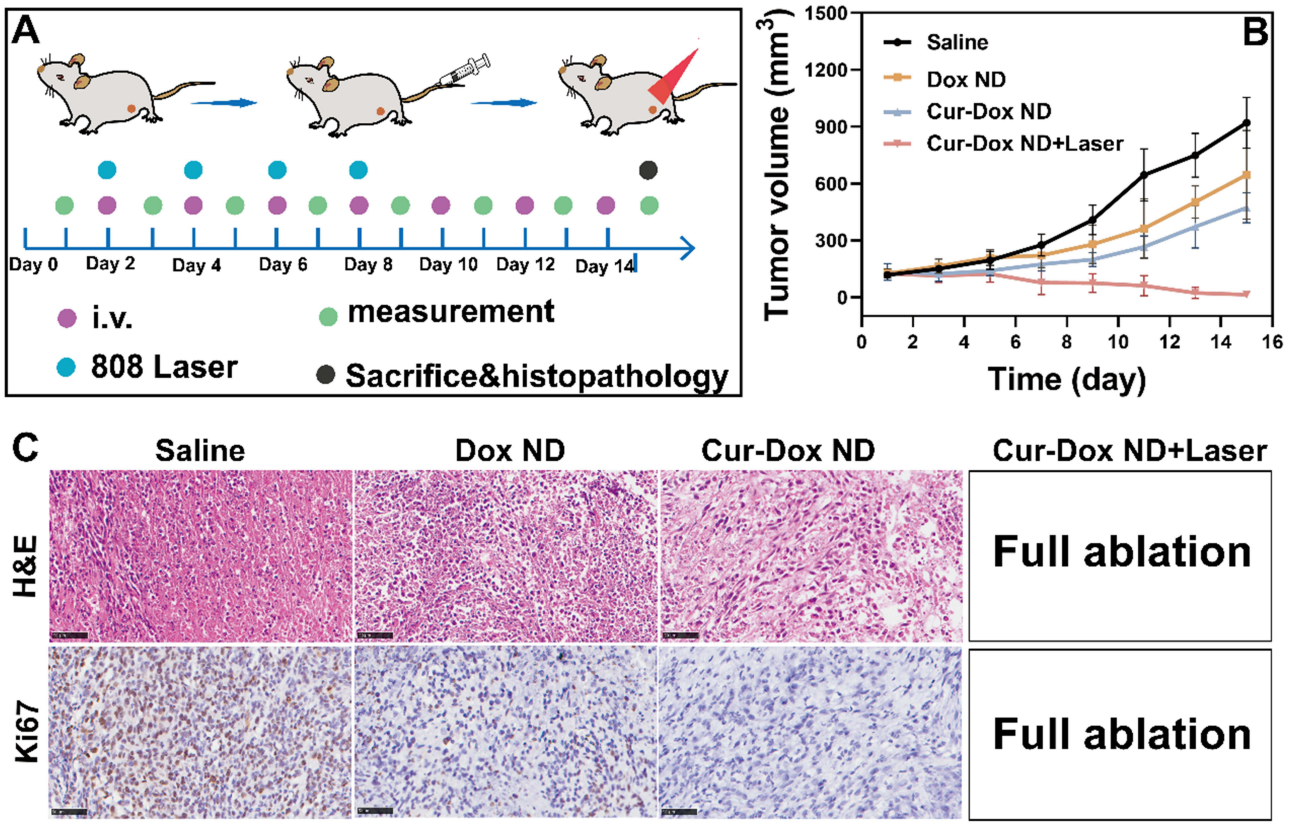

Figure 7 In vivo antitumor assay. (**A**) Experimental treatment scheme. (**B**) Changes of tumor volume in different groups during the treatment cycle. (**C**) H&E staining and Ki67 of the tumor tissue from different groups after the treatment cycle. Scale bar is 50 μm.

In vivo Biosafety

To ensure optimal in vivo efficacy of ND, maintaining an excellent biosafety profile is imperative. To assess the biosafety of Cur-Dox ND, we conducted a hemolysis assay and the results were displayed in Figure S6. The hemolysis values of Cur-Dox ND at Dox concentrations of 3, 6, 12, 24, 48, 96, and 192 μg/mL were comparable to those of the negative control group (PBS), indicating notable blood compatibility of Cur-Dox ND. Furthermore, an MTT assay on NIH3T3 cells revealed that the cell survival rates, when treated with varying concentrations of Cur-Dox ND, were akin to those of the blank control, suggesting minimal toxicity towards normal cells and outstanding biocompatibility (Figure 8A). Throughout the in vivo efficacy experiment, the body weight of mice was monitored every two days. The results demonstrated no significant differences in body weight between the PBS-administered group and the other groups over the 15-day period (Figure 8B). Additionally, H&E staining on major organs revealed no noteworthy abnormalities or injuries in the treated mice across all ND groups (Figure 8C). In summary, these collective findings attest that Cur-Dox ND not only manifests excellent anti-tumorigenic activity but also exhibits remarkable biosafety.

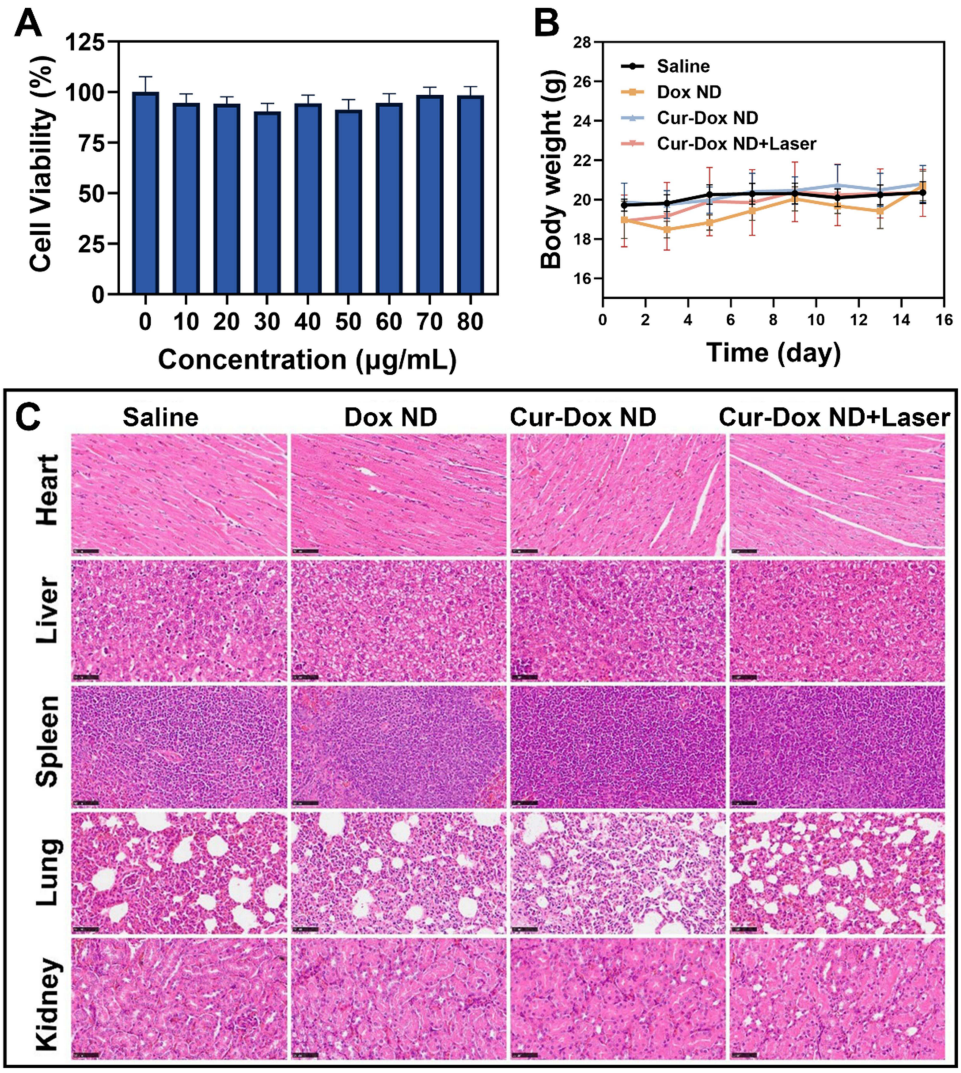

Figure 8 Biosafety assay of Cur-Dox ND. (**A**) Cell viability of NIH3T3 cells treated with different concentrations of Cur-Dox ND for 24 h. (**B**) Changes of body weight in different groups during the treatment cycle. (**C**) H&E staining of major organs from different groups after the treatment cycle. Scale bar is 50 μm.

Conclusion

In summary, here in this study, with the aim to devise an ND platform to overcome the in vivo barriers and MDR of tumors, we first complex Cur and Dox into a well-dispersed ND (Cur-Dox ND) using ferric ion as the linker and PVP as the stabilizer and regulator. It was found that the size of Cur-Dox ND can be conveniently regulated by changing the charge of PVP from ~10 nm to over 100 nm. The selected model Cur-Dox ND with size of ~20 nm showed synergetic chemotherapy effects on 4T1 cells which can reverse the MDR for increased intracellular drug retention. Importantly, Cur-Dox ND can be maintained stable under physiological environments while response to acidic environment to give accelerated but sustainable drug release. Moreover, Cur-Dox ND exerts decent photothermal ability, which is able to further enhance the final anticancer effects to build a multifunctional platform. Upon testing in MCTS model, it was found that Cur-Dox ND can also afford elevated inhibition of 3D tumors, which might be attributed to its superior drug penetration as well as photothermal-enhanced cellular uptake and drug release. At last, the in vivo tumor assay revealed the good tumor targetability and further confirmed the in vivo antitumor performance of Cur-Dox ND.

Declaration of Generative AI and AI-Assisted Technologies in the Writing Process

During the preparation of this work, the authors used ChatGPT (https://chat.openai.com/) in order to improve readability and language. After using this tool/service, the authors reviewed and edited the content as needed and take full responsibility for the content of the publication.

Data Sharing Statement

Data will be made available on request.

Acknowledgments

The authors acknowledge the financial support from Jiangsu Key Research and Development Plan (Society Development (No. BE2022720); Science & Technology Support Program of Changzhou (No. CJ20235037); Natural Science Foundation of Jiangsu Province (No. BK20210851); Major Program of Science and Technology Project of Changzhou Health Commission (No. ZD202021); Postgraduate Research & Practice Innovation Program of Jiangsu Province (No. SJCX231464). The authors acknowledge the tissue slide preparation, staining, and imaging services provided by Record Biological Technology Co., Ltd. (Shanghai, China); the TEM imaging provided by Zhenjiang ZhuanBo Detection Technology Co., Ltd., and animal experiments service provided by Cavens animal center (Changzhou, China).

Disclosure

The authors report no conflicts of interest in this work.

References

1. Ashrafizadeh M, Delfi M, Zarrabi A, et al. Stimuli-responsive liposomal nanoformulations in cancer therapy: pre-clinical & clinical approaches. *J Control Release*. 2022;351:50–80. doi:10.1016/j.jconrel.2022.08.001
2. Dessale M, Mengistu G, Mengist HM. Nanotechnology: a promising approach for cancer diagnosis, therapeutics and theragnosis. *Int j Nanomed*. 2022;17:3735. doi:10.2147/IJN.S378074
3. Hanahan D. Hallmarks of cancer: new dimensions. *Cancer Discovery*. 2022;12(1):31–46. doi:10.1158/2159-8290.CD-21-1059
4. Siegel RL, Miller KD, Wagle NS, Jemal A. Cancer statistics, 2023. *Ca Cancer J Clin*. 2023;73(1):17–48. doi:10.3322/caac.21763
5. Thanki K, Gangwal RP, Sangamwar AT, Jain S. Oral delivery of anticancer drugs: challenges and opportunities. *J Control Release*. 2013;170 (1):15–40. doi:10.1016/j.jconrel.2013.04.020
6. Holohan C, Van Schaeybroeck S, Longley DB, Johnston PG. Cancer drug resistance: an evolving paradigm. *Nat Rev Cancer*. 2013;13(10):714–726. doi:10.1038/nrc3599
7. Chen M, Chen B, Ge X, Ma Q, Gao S. Targeted nanodrugs to destroy the tumor extracellular matrix barrier for improving drug delivery and cancer therapeutic efficacy. *Mol Pharmaceut*. 2023;20(5):2389–2401. doi:10.1021/acs.molpharmaceut.2c00947
8. Duan C, Yu M, Xu J, Li B-Y, Zhao Y, Kankala RK. Overcoming cancer multi-drug resistance (MDR): reasons, mechanisms, nanotherapeutic solutions, and challenges. *Biomed Pharmacother*. 2023;162:114643. doi:10.1016/j.biopha.2023.114643
9. Blanco E, Shen H, Ferrari M. Principles of nanoparticle design for overcoming biological barriers to drug delivery. *Nature Biotechnol*. 2015;33 (9):941–951. doi:10.1038/nbt.3330

10. Curtis LT, Frieboes HB. The tumor microenvironment as a barrier to cancer nanotherapy. *Syst Biol Tumor Microenviron*. 2016;2016:165–190.
11. Kim SM, Faix PH, Schnitzer JE. Overcoming key biological barriers to cancer drug delivery and efficacy. *J Control Release*. 2017;267:15–30. doi:10.1016/j.jconrel.2017.09.016
12. Oberoi RK, Parrish KE, Sio TT, Mittapalli RK, Elmquist WF, Sarkaria JN. Strategies to improve delivery of anticancer drugs across the blood–brain barrier to treat glioblastoma. *Neuro-Oncology*. 2015;18(1):27–36. doi:10.1093/neuonc/nov164
13. Majidinia M, Mirza-Aghazadeh-Attari M, Rahimi M, et al. Overcoming multidrug resistance in cancer: recent progress in nanotechnology and new horizons. *IUBMB Life*. 2020;72(5):855–871. doi:10.1002/iub.2215
14. Park H, Otte A, Park K. Evolution of drug delivery systems: from 1950 to 2020 and beyond. *J Control Release*. 2022;342:53–65. doi:10.1016/j.jconrel.2021.12.030
15. Mitchell MJ, Billingsley MM, Haley RM, Wechsler ME, Peppas NA, Langer R. Engineering precision nanoparticles for drug delivery. *Nat Rev Drug Discov*. 2021;20(2):101–124. doi:10.1038/s41573-020-0090-8
16. Li X, Zhang Y, Ma Z, He C, Wu Y, An Q. Designing cancer nanodrugs that are highly loaded, pH-responsive, photothermal, and possess a favored morphology: a hierarchical assembly of DOX and layer-by-layer modified rGO. *Chin Chem Lett*. 2019;30(2):489–493. doi:10.1016/j.cclet.2018.03.019
17. Barenholz YC. Doxil®—The first FDA-approved nano-drug: lessons learned. *J Control Release*. 2012;160(2):117–134. doi:10.1016/j.jconrel.2012.03.020
18. Chen H, Zhou B, Zheng X, Wei J, Ji C, Yin M. Tumor microenvironment-activated multi-functional nanodrug with size-enlargement for enhanced cancer phototheranostics. *Biomater. Sci.* 2023;11(2):472–480. doi:10.1039/D2BM01604D
19. Wang W, Zhang D, Jiang Z, et al. A Nanodrug-Enabled chemosensitization of cancer stem cells against tumor progression and metastasis. *Chem Eng J*. 2023;477:147121. doi:10.1016/j.cej.2023.147121
20. Nakamura H, Jun F, Maeda H. Development of next-generation macromolecular drugs based on the EPR effect: challenges and pitfalls. *Expert Opin Drug Delivery*. 2015;12(1):53–64. doi:10.1517/17425247.2014.955011
21. Shen Y, Bae YH. Tumour extravasation of nanomedicine: the EPR and alternative pathways. *Adv Drug Delivery Rev*. 2023;194:114707. doi:10.1016/j.addr.2023.114707
22. Wang C, Zhang S. Advantages of nanomedicine in cancer therapy. *A Rev ACS Applied Nano Mater*. 2023;6:22594–22610. doi:10.1021/acsanm.3c04487
23. Wang C. Reconstituted lipid nanoparticles from cells/tissues for drug delivery in cancer. *Mol Pharmaceut*. 2023;20(6):2891–2898. doi:10.1021/acs.molpharmaceut.2c01033
24. Zhang RX, Wong HL, Xue HY, Eoh JY, Wu XY. Nanomedicine of synergistic drug combinations for cancer therapy–Strategies and perspectives. *J Control Release*. 2016;240:489–503. doi:10.1016/j.jconrel.2016.06.012
25. Liu S, Khan AR, Yang X, Dong B, Ji J, Zhai G. The reversal of chemotherapy-induced multidrug resistance by nanomedicine for cancer therapy. *J Control Release*. 2021;335:1–20. doi:10.1016/j.jconrel.2021.05.012
26. Fulfager AD, Yadav KS. Understanding the implications of co-delivering therapeutic agents in a nanocarrier to combat multidrug resistance (MDR) in breast cancer. *J Drug Delivery Sci Technol*. 2021;62:102405. doi:10.1016/j.jddst.2021.102405
27. Wang H, Huang Y. Combination therapy based on nano codelivery for overcoming cancer drug resistance. *Med Drug Discov*. 2020;6:100024. doi:10.1016/j.medidd.2020.100024
28. Liu S, Li R, Qian J, et al. Combination therapy of doxorubicin and quercetin on multidrug-resistant breast cancer and their sequential delivery by reduction-sensitive hyaluronic acid-based conjugate/d-α-tocopheryl poly (ethylene glycol) 1000 succinate mixed micelles. *Mol Pharmaceut*. 2020;17(4):1415–1427. doi:10.1021/acs.molpharmaceut.0c00138
29. Gao Q, Feng J, Liu W, et al. Opportunities and challenges for co-delivery nanomedicines based on combination of phytochemicals with chemotherapeutic drugs in cancer treatment. *Adv Drug Delivery Rev*. 2022;188:114445. doi:10.1016/j.addr.2022.114445
30. Zong L, Cheng G, Liu S, Pi Z, Liu Z, Song F. Reversal of multidrug resistance in breast cancer cells by a combination of ursolic acid with doxorubicin. *J Pharmac Biomed Analy*. 2019;165:268–275. doi:10.1016/j.jpba.2018.11.057
31. Wang H, Zhou J, Fu Y, et al. Deeply infiltrating iRGD-graphene oxide for the intensive treatment of metastatic tumors through PTT-mediated chemosensitization and strengthened integrin targeting-based antimigration. *Adv. Healthcare Mater*. 2021;10(16):2100536. doi:10.1002/adhm.202100536
32. Wang C, Chen S, Yu F, et al. Dual-channel theranostic system for quantitative self-indication and low-temperature synergistic therapy of cancer. *Small*. 2021;17(10):2007953. doi:10.1002/smll.202007953
33. Geng S, Zhao H, Zhan G, Zhao Y, Yang X. Injectable in situ forming hydrogels of thermosensitive polypyrrole nanoplatforms for precisely synergistic photothermo-chemotherapy. *ACS Appl Mater Interfaces*. 2020;12(7):7995–8005. doi:10.1021/acsami.9b22654
34. Niu C, Xu Y, An S, et al. Near-infrared induced phase-shifted ICG/Fe3O4 loaded PLGA nanoparticles for photothermal tumor ablation. *Sci Rep*. 2017;7(1):5490. doi:10.1038/s41598-017-06122-1
35. Zhang X, Ma Y, Zhang X, Pang X, Yang Z. Bio-inspired self-assembled bacteriochlorin nanoparticles for superior visualization and photothermal ablation of tumors. *Biomed Pharmacother*. 2023;165:115014. doi:10.1016/j.biopha.2023.115014
36. Dai X, Li L, Li M, et al. One pot preparation of muti-mode nanoplatform to combat ovarian cancer. *Biomed Pharmacother*. 2023;165:115172. doi:10.1016/j.biopha.2023.115172
37. Liu R, Luo C, Pang Z, et al. Advances of nanoparticles as drug delivery systems for disease diagnosis and treatment. *Chin Chem Lett*. 2023;34(2):107518. doi:10.1016/j.cclet.2022.05.032
38. Gavas S, Quazi S, Karpiński TM. Nanoparticles for cancer therapy: current progress and challenges. *Nanoscale Res Lett*. 2021;16(1):173. doi:10.1186/s11671-021-03628-6
39. Chen S, Wang Z, Liu L, et al. Redox homeostasis modulation using theranostic AIE nanoparticles results in positive-feedback drug accumulation and enhanced drug penetration to combat drug-resistant cancer. *Mater Today Bio*. 2022;16:100396. doi:10.1016/j.mtbio.2022.100396
40. Chang Y, Cui P, Zhou S, et al. Metal-phenolic network for cancer therapy. *J Drug Delivery Sci Technol*. 2023;81:104194. doi:10.1016/j.jddst.2023.104194
41. Wang C, Chen S, Bao L, Liu X, Hu F, Yuan H. Size-controlled preparation and behavior study of phospholipid–calcium carbonate hybrid nanoparticles. *Int J Nanomed*. 2020;Volume 15:4049–4062. doi:10.2147/IJN.S237156

42. Hoshyar N, Gray S, Han H, Bao G. The effect of nanoparticle size on in vivo pharmacokinetics and cellular interaction. *Nanomedicine*. 2016;11(6):673–692. doi:10.2217/nnm.16.5
43. Keyvani-Ghamsari S, Khorsandi K, Gul A. Curcumin effect on cancer cells' multidrug resistance: an update. *Phytother Res*. 2020;34(10):2534–2556. doi:10.1002/ptr.6703
44. Sagnou M, Novikov FN, Ivanova ES, et al. Novel curcumin derivatives as P-glycoprotein inhibitors: molecular modeling, synthesis and sensitization of multidrug resistant cells to doxorubicin. *Eur J Med Chem*. 2020;198:112331. doi:10.1016/j.ejmech.2020.112331
45. Chan LL-Y, McCulley KJ, Kessel SL. Assessment of cell viability with single-, dual-, and multi-staining methods using image cytometry. *Cell Viability Assays*. 2017;2017:27–41.
46. Mirzaei S, Gholami MH, Hashemi F, et al. Advances in understanding the role of P-gp in doxorubicin resistance: molecular pathways, therapeutic strategies, and prospects. *Drug Discovery Today*. 2022;27(2):436–455. doi:10.1016/j.drudis.2021.09.020
47. Chen S-Q, Wang C, Song Y-Q, et al. Quercetin covalently linked lipid nanoparticles: multifaceted killing effect on tumor cells. *ACS omega*. 2020;5(46):30274–30281. doi:10.1021/acsomega.0c04795
48. Kunjachan S, Błauż A, Möckel D, et al. Overcoming cellular multidrug resistance using classical nanomedicine formulations. *Eur J Pharm Sci*. 2012;45(4):421–428. doi:10.1016/j.ejps.2011.08.028
49. Mura S, Nicolas J, Couvreur P. Stimuli-responsive nanocarriers for drug delivery. *Nature Mater*. 2013;12(11):991–1003. doi:10.1038/nmat3776
50. Yin Q, Shen J, Zhang Z, Yu H, Li Y. Reversal of multidrug resistance by stimuli-responsive drug delivery systems for therapy of tumor. *Adv Drug Delivery Rev*. 2013;65(13–14):1699–1715. doi:10.1016/j.addr.2013.04.011
51. Kulshrestha A, Katara GK, Schneiderman S, et al. Targeting the pH regulators in the tumor microenvironment for ovarian cancer treatment. *Clin Cancer Res*. 2020;26(13):113. doi:10.1158/1557-3265.OVCA19-B64
52. Savic LJ, Schobert IT, Peters D, et al. Molecular imaging of extracellular tumor pH to reveal effects of locoregional therapy on liver cancer microenvironment. *Clin Cancer Res*. 2020;26(2):428–438. doi:10.1158/1078-0432.CCR-19-1702
53. Karimi M, Eslami M, Sahandi-Zangabad P, et al. pH-Sensitive stimulus-responsive nanocarriers for targeted delivery of therapeutic agents. *Wiley Interdiscip Rev Nanomed Nanobiotechnol*. 2016;8(5):696–716. doi:10.1002/wnan.1389
54. Fang W, Yang J, Gong J, Zheng N. Photo- and pH-triggered release of anticancer drugs from mesoporous silica-coated. *Pd@Ag Nanoparticles*. 2012;22(4):842–848.
55. Liu X, Wang C, Ma H, Yu F, Hu F, Yuan H. Water-responsive hybrid nanoparticles codelivering ICG and DOX effectively treat breast cancer via hyperthermia-aided DOX functionality and drug penetration. *Adv. Healthcare Mater*. 2019;8(8):1801486. doi:10.1002/adhm.201801486
56. Bhatt HN, Diwan R, Borrego EA, et al. A photothermal driven chemotherapy for the treatment of metastatic melanoma. *J Control Release*. 2023;361:314–333. doi:10.1016/j.jconrel.2023.08.005
57. Lu H, Stenzel MH. Multicellular tumor spheroids (MCTS) as a 3D in vitro evaluation tool of nanoparticles. *Small*. 2018;14(13):1702858. doi:10.1002/smll.201702858
58. Wang C, Wang Z, Chen S, et al. Modulation of aggregation-caused quenching to aggregation-induced emission: finding a biocompatible polymeric theranostics platform for cancer therapy. *Macromol Rapid Communic*. 2021;42(19):2100264. doi:10.1002/marc.202100264
59. Yu J, Wang L, Xie X, et al. Multifunctional nanoparticles codelivering doxorubicin and amorphous calcium carbonate preloaded with indocyanine green for enhanced chemo-photothermal cancer therapy. *Int J Nanomed*. 2023;Volume 18:323–337. doi:10.2147/IJN.S394896
60. Zhou J, Li K, Zang X, Xie Y, Song J, Chen X. Ros-responsive galactosylated-nanoparticles with doxorubicin entrapment for triple negative breast cancer therapy. *Int J Nanomed*. 2023;Volume 18:1381–1397. doi:10.2147/IJN.S396087
61. Xiong H, Wang C, Wang Z, Lu H, Yao J. Self-assembled nano-activator constructed ferroptosis-immunotherapy through hijacking endogenous iron to intracellular positive feedback loop. *J Control Release*. 2021;332:539–552. doi:10.1016/j.jconrel.2021.03.007